water

MDPI

Article

Spatiotemporal Assessment of Soil Erosion Under Historical and Projected Land-Use Scenarios in the Myjava Basin, Slovakia

Aditya Nugraha Putra, Roman Výleta, Michaela Danáčová, Kamila Hlavčová and Silvia Kohnová *

Department of Land and Water Resources Management, Faculty of Civil Engineering, Slovak University of Technology in Bratislava, Radlinského 11, 810 05 Bratislava, Slovakia
* Correspondence: silvia.kohnova@stuba.sk; Tel.: +421-2-32-888-623

Abstract

Soil erosion remains a critical global concern, yet long-term catchment-scale assessments that explicitly link historical land-use transitions with erosion responses remain limited. This study evaluates how ±240 years record of historical and projected land-use changes influence soil erosion in the Myjava Basin by integrating parcel-level land-use reconstructions from 1787 to 2030 into a distributed USLE-2D framework. R, K, and parcel-based C and P factors were temporally standardized, and LS was derived using an ensemble of four widely applied algorithms. A PCA was applied to quantify the relative contribution of RUSLE factors across time, and all analyses were performed within a reproducible geospatial modelling environment. The results indicated a long-term decline in total erosion of ±78% at the landscape scale and ±60% within arable land from the 19th century to the present, driven mainly by a major reduction in arable land (from ±62% to ±37%) and expansion of forest and shrub vegetation. Despite this decline, persistent hotspots remain concentrated on steep upland slopes with high LS (>10%), while agricultural parcels experienced erosion rates 10–20 times higher than the basin-wide mean across all periods. PCA shows that LS and rainfall erosivity dominate erosion variability (PC loadings ±0.78–0.84), while C and P factors increase in influence in recent and projected periods, contributing up to ±40% of total explained variance. These findings demonstrate that long-term land-use transitions have substantially reduced basin-scale erosion risk.

Keywords: Myjava Basin; soil erosion modelling; land-use change; spatiotemporal analysis; catchment-scale assessment

1. Introduction

Across centuries, soil erosion by water has quietly sculpted the Earth's surface, not only as a geomorphic process but also as a testimony of how societies have interacted with land. Contemporary assessments show that the rate of soil loss now surpasses the pace of its natural regeneration, creating long-term ecological consequences with direct implications for land management [1]. Global-scale modelling efforts, such as the GloSEM framework, estimate that human-induced soil displacement had already reached about 35.9 Pg yr^{-1} by 2012, roughly 2.5% higher than in 2001, underscoring the cumulative legacy of intensive cultivation, deforestation, and land degradation [2]. Future projections coupling socio-economic and climatic movements warn of a potential 30–66% escalation by mid-century [3], highlighting erosion as both a physical process and a socio-ecological outcome shaped by land-use decisions. In spite of these global assessments, long-term catchment-scale

Academic Editor: Chin H Wu

Received: 9 December 2025
Revised: 3 January 2026
Accepted: 15 January 2026
Published: 18 January 2026

evaluations, particularly in central Europe, remain limited, leaving important questions about how historical land-use directions shape erosion responses over time.

Building on the historical cartographic analyses of [4] and the extended reconstructions by [5] spanning 1787–2010, which jointly documented the long-term transformation of the Myjava landscape from forest-dominated terrain to intensively cultivated farmland, historical and projected land-use maps of the Myjava watershed (1787–2030) were developed using an Artificial Neural Network–Cellular Automata–Markov Chain (ANN–CA–Markov) framework. The reconstructed land-use sequences indicate a gradual reduction in arable land over time, accompanied by the abandonment of marginal agricultural areas and progressive reforestation. The landscape has shifted between phases of agricultural expansion and natural regeneration, shaped by both past land-use and ecological processes. These land-use trajectories are consistent with long-term patterns identified in previous historical reconstructions [5,6], indicating a clear shift in the landscape's structural and ecological configuration. However, previous land-use modelling efforts did not assess how these transitions influence soil erosion processes. In parallel, soil erosion in Slovakia has been extensively investigated through national-scale assessments and field-based studies in small agricultural catchments, including the Myjava region, demonstrating the influence of crop management, sediment connectivity, and reservoir sedimentation on erosion and sediment transport [7–10]. However, these studies are largely constrained to short- to medium-term analyses and do not explicitly resolve how multi-century land-use trajectories condition present and future erosion responses at the parcel scale. This unaddressed link inspired the present study to evaluate the relationship between land-use transitions and erosion responses across space and time. This study presents a parcel-level, multi-century ($\pm$240 years) assessment of soil erosion that integrates historical and projected land-use dynamics. The combined application of USLE-2D and PCA provides a novel approach to attribute long-term erosion responses to evolving land-use controls.

Reliable and chronologically consistent land-use records form the backbone of erosion modelling, as they delineate how vegetation cover, roughness, and management practices mediate sediment detachment and transport [11–14]. When mapped at the parcel scale, such datasets capture fine-grained heterogeneity in land management and boundary transitions between agricultural, forested, and semi-natural areas, which are critical for quantifying the spatial distribution of erosion risk. Temporal sequences of land-use change also provide dynamic inputs for calculating the cover management (C) and support practice (P) factors within the USLE framework, allowing erosion responses to be linked directly to land-use directions [13,14]. Long-term, parcel-level land-use datasets therefore provide a valuable foundation for assessing how landscape transformations influence erosion susceptibility over time. Consequently, temporally validated land-use information, such as that reconstructed by [6] and [5], is indispensable for developing robust erosion monitoring systems in dynamic landscapes like the Myjava Basin. The Myjava Basin, with its steep cultivated slopes and long history of land-use restructuring, presents an especially valuable setting for examining these interactions.

In soil erosion modelling, land-use acts as the dominant control shaping the spatiotemporal variability of the cover management (C) and support practice (P) factors, which together define the protective capacity of the landscape against soil detachment and transport. Parcel-based land-use information enables explicit representation of agricultural practices, vegetation density, and conservation structures, allowing realistic estimation of C–P dynamics under changing land management regimes. Historical and projected land-use sequences, such as those available for the Myjava Basin, provide a unique opportunity to examine how long-term transformations, from intensive cultivation to gradual reforestation, translate into measurable shifts in C and P parameters. This temporal continuity

allows erosion to be interpreted not as a static outcome but as an evolving geomorphic response to human land-use decisions. The main objective of this research is to assess how historical and projected land-use transitions control soil erosion across space and time in the Myjava region at the basin and parcel scales by integrating multi-century land-use reconstructions into a distributed USLE-2D soil erosion modelling framework. It is hypothesized that land-use transitions will produce detectable changes in erosion magnitude and spatial patterns, while long-term geomorphological controls remain persistent, with the magnitude and spatial distribution of soil loss reflecting the evolving land-use across the landscape from the late 18th century to projected future conditions.

2. Materials and Methods

2.1. Study Area

The Myjava sub-basin in western Slovakia represents a characteristic hilly agro-landscape of the Outer Western Carpathians, where a long history of cultivation and deforestation has intensified susceptibility to water erosion. Covering an area of about 644 km^2 between 48°40′ and 48°50′ N and 17°10′ and 17°40′ E (Figure 1), the basin ranges in elevation from 167 to 795 m a.s.l. The region experiences a temperate climate, with mean annual precipitation of 650–800 mm and average temperatures between 7 and 9 °C [4]. The prevailing soil types are Cambisols and Luvisols, which are moderately deep but prone to erosion on slopes steeper than 7°, a condition that elevates erosion susceptibility and supports the application of spatially distributed models such as USLE-2D [6].

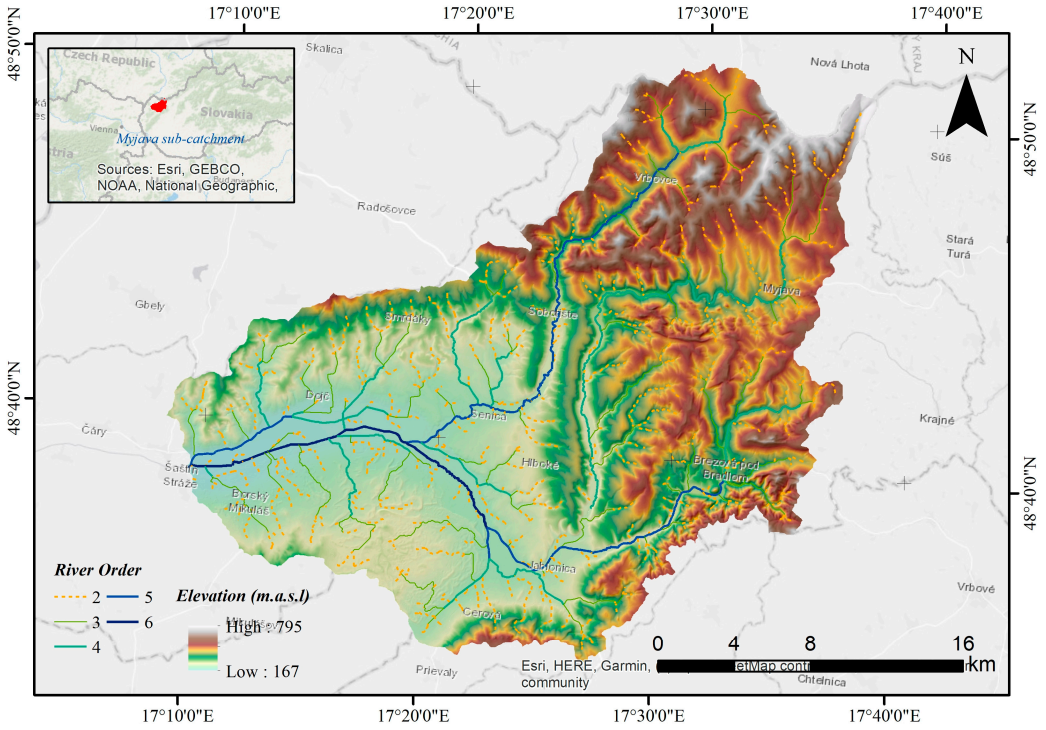

Figure 1. Geographical location, elevation gradient, and river network of the Myjava Basin.

The basin's land-use has undergone pronounced transformation since the late eighteenth century, profoundly altering surface runoff patterns and sediment dynamics over time. The basin's land-use history reflects a long-term transition from predominantly forested terrain in the late 18th century toward intensified agricultural expansion during the 19th and early 20th centuries, followed by gradual abandonment of marginal croplands and recovery of forest and shrub vegetation, creating a mosaic of forests, grasslands, and arable fields [15], a trajectory consistent with previous historical reconstructions and central

to interpreting long-term erosion responses. Hydrologically, the sub-basin drains into the Myjava River, a tributary of the Morava, and exhibits flashy runoff behaviour characteristic of dissected uplands, affecting the spatial distribution of soil erosion simulated using the USLE-2D model. The USLE-2D framework applied in this study estimates long-term average soil erosion rather than event-based losses; therefore, the analysis focuses on relative spatial and temporal patterns of erosion dynamics rather than on absolute erosion magnitudes. The long-term human imprint combined with steep topography creates favourable conditions for analyzing how centuries of land-use transitions modulate soil erosion risk, particularly when evaluated through dynamic R, K, LS, C, and P factors derived from spatial modelling.

2.2. Land-Use Data Sources and Processing

Five land-use datasets were utilized, including historical maps from 1787, 1865, and 1957, a remote-sensing-based map for 2010 and 2025C (classified from Sentinel-2A using random forest analysis), complemented by two future projections for 2025P and 2030 (generated using an Artificial Neural Network–Cellular Automata–Markov Chain (ANN–CA–Markov) modelling framework applied to the Myjava Basin). The historical maps originate from the First Military Survey (1764–1787) and Second Military Survey (1819–1869), produced at a nominal scale of approximately 1:28,800, and mid-20th-century topographic maps at a scale of approximately 1:25,000, following standard Slovak cartographic documentation. Historical maps were rasterized, georeferenced to the S-JTSK coordinate system using stable landscape features such as settlement cores, road intersections, and river confluences, and standardized into the following two unified classes: arable land and non-arable land (including broad-leaf forest, coniferous forest, mixed forest, natural grassland, transitional shrub, and urbanized areas), following a harmonized land-use classification scheme designed to ensure temporal consistency across historical and contemporary datasets. Georeferencing accuracy is inherently lower for the earliest maps due to the absence of a geodetic control network and minor positional uncertainty is expected, particularly along arable–non-arable boundaries. To reduce classification bias, land-use was aggregated into two broad classes, so that potential boundary errors primarily affect local absolute estimates rather than relative spatial and temporal patterns. Model validation of the land-use classification and projection models showed high reliability, with overall accuracy exceeding 93%, Kappa above 0.88, and Khist consistently > 0.95. These accuracy metrics were derived from internal validation procedures, including cross-validation for the random forest classifications and hindcasting-based validation for the ANN–CA–Markov projections. Residual errors in the land-use projection results were mainly confined to ecotone transitions between cropland, grassland, and woodland, reflecting fine-scale heterogeneity that produced minor spatial displacement (Kloc 0.89–0.91). The ANN–CA–Markov model was validated using a hindcasting approach, whereby historical land-use transitions were simulated and compared against observed land-use maps. Model performance was evaluated using overall accuracy, Kappa coefficient, Khist, and Kloc metrics, indicating high agreement between simulated and observed land-use patterns. Because future land-use states cannot be directly validated, the reliability of the 2025P and 2030 projections is inferred from the strong performance of the model in reproducing historical land-use changes.

2.3. Rainfall-Runoff Erosion Factor (R Factor)

The rainfall erosivity factor (R) for the Myjava Basin was derived from an altitude layer of the Slovak Republic (25 × 25 m resolution) generated from a TIN digital relief model based on Seamless Vector Map 50 (SVM 50) height data (10 m intervals) [16]. Additional

datasets included climatic region and mean annual precipitation maps from the Atlas of the Slovak Republic [17,18], complemented by 86 ombrographic stations containing R factor values previously calculated by [19]. These layers were integrated and spatially overlaid to generate the R factor map. Ref. [20] updated the erosive rainfall factor for Slovakia using long-term pluviographic datasets, providing an improved regional basis for R factor estimation. Through visual interpretation and expert validation, representative R factor values were assigned to each polygon to represent erosivity across contrasting topographic and climatic zones. The resulting R factor map reflects spatial variability in rainfall erosivity associated with altitude and climatic zonation. A stationary R-factor layer based on long-term climatic averages was applied for the historical periods (1787–1869), while an updated R factor layer derived from recent pluviographic data was used for the modern and projected periods (1957–2030).

For the earliest historical periods, direct rainfall observations are unavailable; therefore, the use of a stationary R factor follows established Slovak erosion studies and was adopted to isolate land-use-driven erosion responses rather than uncertain historical climate variability. This assumption may affect absolute erosion values but does not alter relative spatial or temporal patterns derived under a consistent erosivity framework. The R factor was not modified by climate change projections for 2030; thus, differences among scenarios primarily reflect land-use dynamics rather than climatic forcing.

2.4. Soil Erodibility Factor (K Factor)

The soil erodibility factor (K) was compiled from Slovakia's official soil units (Bonitované pôdno-ekologické jednotky or BPEJ) published as open data, which provide polygonal delineations of agronomic–ecological units at national scale (data.slovensko.sk). The BPEJ layer was first checked and refined against a 10 m resolution Digital Elevation Model (DEM) to sharpen polygon boundaries via on-screen digitizing where legacy edges deviated from terrain breaks. Each BPEJ polygon was then attributed with a K value using the nationally applied lookup table commonly used in Slovakia for USLE/RUSLE applications and joined by the BPEJ code; the attributed polygons were finally rasterized to the same grid as the DEM to ensure cell-to-cell alignment with other USLE-2D inputs. This workflow follows current practice for deriving K from texture/organic matter-based nomograph relations while remaining compatible with recent European/global advances in K mapping.

2.5. Slope Length–Steepness Factor (LS Factor)

The LS factor map was generated through a structured multi-step process to ensure spatial consistency and accuracy across different historical and projected land-use scenarios. First, the DEM was exported to ASCII format and reconverted to raster (.rst) using the LS Converter 1.0 tool to maintain the original grid resolution and coordinate reference. A single high-resolution DEM was used for all time slices, assuming that catchment-scale topographic configuration remains structurally stable over the study period and serves as a persistent geomorphic template for erosion processes. Subsequently, parcel maps representing land management units and crop information were prepared for each target year (1787, 1869, 1957, 2010, 2025C, 2025P, and 2030). Each parcel was clipped to include only arable land, assigned a unique parcel ID, and rasterized to ensure consistency with the DEM's resolution and extent. Potential micro-scale topographic modifications (e.g., gully development, terracing, or local sediment redistribution) could not be explicitly reconstructed due to the absence of reliable historical elevation data and were therefore not represented in the LS factor.

The land-use parcel rasters were transformed into ASCII and reconverted into .rst format using the LS Converter for compatibility with the LS computation module. The

final computation of the slope length–steepness factor (LS) was performed in USLE-2D using four independent algorithms, [20–23] each representing different parameterizations of slope gradient and flow accumulation. The four LS outputs were then averaged cell by cell to derive a representative mean LS value for each temporal scenario. This ensemble approach reduced methodological bias across algorithms and improved robustness in representing complex topographic effects on erosion potential. The resulting LS maps ensured consistent alignment, reproducibility, and comparability across all historical and projected datasets, forming a solid foundation for subsequent USLE-2D soil loss modelling.

1. Ref. [21]: Original USLE formulation is the classical foundation of USLE that is most suitable for gentle to moderate slopes. However, it tends to overestimate erosion on steep terrains because flow accumulation is not explicitly included.

$$LS_{Wischmeier} = (\frac{\lambda}{22.13})^{m} \times (65.41\sin^2\theta + 4.56\sin\theta + 0.065) \quad (1)$$

Description:

- λ = slope length (m);
- θ = slope angle (degrees);
- m = variable exponent (0.2–0.5) depending on slope gradient;
- $m = 0.2$ for slope < 1%;
- $m = 0.3$ for 1–3%;
- $m = 0.4$ for 3–5%;
- $m = 0.5$ for >5%.

2. Ref. [22]: Flow accumulation-based formulation introduced by Govers uses of specific catchment area (A_s) to represent actual flow length instead of a fixed slope length. It performs well on complex or convergent slopes and is less sensitive to local DEM irregularities, making it ideal for distributed models like USLE-2D.

$$LS_{Govers} = (\frac{A_s}{22.13})^{0.4} \times (\frac{\sin\theta}{0.0896})^{1.3} \quad (2)$$

Description:

- A_s = upslope contributing area per unit contour width (m^2/m);
- θ = slope angle (radians).

3. Ref. [23]: Revised slope function (RUSLE adaptation); this modification improves accuracy for moderate to steep slopes, reducing the overestimation tendencies of the original Wischmeier formulation. It was later adopted in RUSLE [24] and remains a standard in many GIS-based implementations.

$$LS_{McCool} = (\frac{\lambda}{22.13})^{m} \times (10.8\sin\theta + 0.03) \quad (3)$$

Description:

- Same variable definitions as Wischmeier and provides a smoother response to steepness compared to the 1978 version.

4. Ref. [25]: Continuous slope function for extreme gradients. Nearing proposed a single continuous function that maintains physical realism for slopes exceeding 20°. It corrects discontinuities between moderate and steep classes, providing more sta-

ble LS estimates under extreme terrain conditions found in hilly catchments and dissected uplands.

$$LS_{Nearing} = (\frac{\lambda}{22.13})^m \times (16.8\sin\theta - 0.5) \quad (4)$$

Description:

- λ and θ as defined previously.

In this research, the four LS formulations were computed independently for each cell using USLE-2D, then averaged to produce a composite LS raster:

$$LS_{mean} = \frac{LS_{Wischmeier} + LS_{Govers} + LS_{McCool} + LS_{Nearing}}{4} \quad (5)$$

This ensemble approach minimizes structural bias among models and captures both flow convergence (Govers) and gradient-dependent (Wischmeier/McCool/Nearing) effects, ensuring robust topographic representation across the study area.

Ref. [26] highlighted that DEM resolution can substantially influence LS-based erosion modelling, especially in dissected hilly terrains. Similar sensitivity to DEM resolution in slope-dependent erosion parameters was also reported by [27], underscoring the importance of topographic detail. Ref. [27] further demonstrated that USLE-based erosion outputs vary significantly with DEM resolution, reinforcing the need for careful selection of terrain data.

2.6. Cover Management and Support Practice Factor (CP Factor)

The cover management (C) and support practice (P) factors were defined for each parcel and year using the same time-sliced parcel maps (1787–2030). Each polygon carried a crop or land-use attribute that was linked to the Slovak USLE lookup table of crop-specific C values (commonly denoted c_p in national guidelines). Values followed the standard classification, e.g., 0.005 for permanent grassland, 0.02 for alfalfa, 0.15 for winter wheat, 0.35 for potatoes, and up to 0.60 used for maize for silage, and were joined to the parcel polygons before rasterising to the 10 m DEM grid so that all USLE-2D inputs shared identical cell alignment.

The P factor was attributed to the same grid according to the presence of conservation practices recorded or inferred in the parcel dataset (contour tillage, strip cropping, and terracing). Where no practice was indicated, P = 1.0 was assumed; parcels with soil conservation measures received lower P values following the national USLE recommendations ($0 < P \leq 1$). The resulting C and P rasters were produced for each historical and projected year and co-registered with the DEM, K, and LS layers to ensure spatial consistency across inputs to the USLE-2D model. Comparable C–P assignment frameworks are widely used in central European erosion studies [1,2]. Ref. [28] emphasizes that although USLE/RUSLE is widely applied, its reliability depends strongly on how land cover and management data are parameterized, particularly when used in heterogeneous agricultural landscapes. The simplification of historical land-use classes into arable and non-arable categories was therefore applied to ensure temporal consistency across heterogeneous historical sources, while crop-specific and land-cover-specific C and P values were still assigned at the parcel level using national Slovak USLE lookup tables. This approach preserves functional differences in vegetation cover and management relevant to erosion processes, while avoiding artificial detail not supported by historical records.

2.7. Soil Erosion Calculation

Annual soil loss (A) for each temporal scenario was estimated using the Universal Soil Loss Equation in its distributed form:

$$A = R \times K \times L \times S \times C \times P \quad (6)$$

where A is the mean annual soil loss (t ha^{-1} yr^{-1}), R represents rainfall erosivity (MJ mm ha^{-1} h^{-1} yr^{-1}), K denotes soil erodibility (t ha h ha^{-1} MJ^{-1} mm^{-1}), L and S correspond to slope length and steepness factors, C is the cover management factor, and P is the support practice factor.

All parameters were prepared as co-registered raster layers with a 10 m grid resolution to maintain spatial consistency. The R and K factors were derived from long-term climatic records and national soil databases, while the LS factor was calculated in USLE-2D using four algorithms, [20–23], which were averaged to produce a composite LS surface. The C and P factors were assigned to each parcel according to land-use and management attributes for every target year (1787, 1869, 1957, 2010, 2025C, 2025P, and 2030). Roads and river buffers were masked to remove non-eroding areas. The resulting A maps represent the spatial distribution of potential soil loss for each time slice, and zonal statistics were used to summarize mean and maximum erosion rates per parcel and sub-basin.

2.8. Principal Component Analysis (PCA) Computation

PCA was applied to the standardized dataset to reduce dimensionality and identify the latent structure governing soil erosion variability across all time periods. Because the RUSLE factors exhibit different units and magnitudes, all inputs were normalized using z-score transformation prior to decomposition. The first two principal components consistently captured the majority of the variance (>60%), reflecting the dominant geomorphological–climatic gradient (driven primarily by LS and R) and a secondary biophysical–management gradient (influenced by K, C, and P). Component scores for all pixels were exported as georeferenced maps (PC1–PC5), allowing spatial interpretation of the major environmental gradients that shape erosion susceptibility across historical and projected land-use conditions [28,29].

2.9. Factor Loadings, Dominant Drivers, and Combined Influence Mapping

Factor loadings were extracted to quantify the contribution of each RUSLE factor to each principal component. The highest absolute loading within a component was used to determine the dominant factor shaping that mode of variability. To evaluate the integrated role of each factor across all components, absolute loadings were weighted by the variance explained, producing a global influence index for R, K, LS, C, and P. A pixel-level dominant factor map was then generated by combining PCA scores with loadings, enabling spatial delineation of areas where erosion is primarily controlled by rainfall, slope processes, soil erodibility, vegetation cover, or land management practices. The PCA biplot provided additional insight by jointly visualizing sample distribution and directional influence of each factor, providing a compact diagnostic tool for interpreting system behaviour across all temporal layers [24,30].

3. Results

3.1. Land-Use Change Dynamics (1787–2030)

Land-use in the Myjava sub-basin has exhibited a dynamic trajectory over the past two centuries, transitioning from an agriculture-dominated landscape toward a more heterogeneous mosaic of forest, shrub, and semi-natural covers (Table 1). In 1787, arable land

occupied approximately 39,700 ha (62%), reflecting the historical dominance of intensive cultivation. Over the following century, land diversification increased, with the emergence of broad-leaf forests (24%) and natural grasslands (15%), while mixed forests declined noticeably. By 1957, agricultural land remained extensive (34,718 ha or 54%), although still lower than its 1787 peak, coinciding with widespread deforestation and increased landscape exposure. The subsequent decades (1957–2010) marked a gradual ecological recovery, as reforestation, grassland restoration, and the spread of transitional shrubs compensated for declining cropland. Between 2010 and the predicted 2030 scenario, land-use became more evenly distributed across classes, with forests (broad-leaf and coniferous combined) stabilizing around 38%, shrubs expanding to ±11%, and urbanized areas increasing modestly to ±4%, indicating continuing peri-urbanization and fragmentation in valley zones.

Table 1. Land-use change dynamics in Myjava Basin (1787–2030).

LULC Type	1787		1869		1957		2010		2025C		2025P		2030	
	ha	**%**	**ha**	**%**	**ha**	**%**	**ha**	**%**	**ha**	**%**	**ha**	**%**	**ha**	**%**
AL	39,673	**62%**	34,709	**54%**	34,718	**54%**	29,473	**46%**	25,225	**39%**	24,093	**37%**	23,801	**37%**
BLF	0	**0%**	15,701	**24%**	6631	**10%**	14,252	**22%**	16,374	**25%**	15,914	**25%**	16,761	**26%**
CF	0	**0%**	0	**0%**	7418	**12%**	6108	**9%**	5612	**9%**	6,27	**10%**	7919	**12%**
MF	14,037	**22%**	0	**0%**	2879	**4%**	1633	**3%**	1164	**2%**	2027	**3%**	0262	**0%**
NG	8895	**14%**	9706	**15%**	5727	**9%**	7756	**12%**	6958	**11%**	7214	**11%**	6402	**10%**
TWS	0	**0%**	2489	**4%**	3468	**5%**	2251	**3%**	7149	**11%**	6809	**11%**	6879	**11%**
UA	1723	**3%**	1722	**3%**	3486	**5%**	2855	**4%**	1846	**3%**	2001	**3%**	2303	**4%**
Total	64.328 ha													

Note: AL: arable lands; BLF: broad-leaf forests; CF: coniferous forests; MF: mixed forests; NG: natural grasslands; TWS: transitional woodland shrubs; and UA: urbanized areas.

Among all land-use categories, arable land experienced the most significant and persistent decline throughout the study period, illustrating a fundamental reversal in land-use priorities. From its peak of 39,673 ha (62%) in 1787, the extent of cultivated land steadily decreased to 29,473 ha (46%) by 2010, and further to 23,801 ha (37%) by 2030 in the projected scenario. This consistent contraction reflects the cumulative effects of rural depopulation, declining agricultural profitability, and reforestation programmes introduced after the socialist collectivization era. The land-use projection reinforces this trend, showing similar reductions in both the classified 2025C (39%) and predicted 2025P (37%) scenarios, with minimal deviation, demonstrating the internal consistency of the modelling framework.

3.2. Land Parcel

To enable parcel-level erosion analysis, the land-use layers for each temporal snapshot (1787, 1869, 1957, 2010, 2025C, 2025P, and 2030) were spatially intersected with the arable land polygons, generating a series of discrete land parcels representing the smallest management units within cultivated areas. Each polygon was assigned a unique parcel ID, allowing direct linkage between spatial features and their corresponding land-use attributes, erosion factors (C and P), and temporal identifiers. This approach produced a consistent geodatabase that enabled parcel tracking across all temporal layers, facilitating temporal comparison and change detection. The resulting parcel-based maps visualize the spatial heterogeneity of cultivated lands across time, highlighting areas of persistence, conversion, and abandonment. Such a detailed spatial framework supports more accurate quantification of erosion dynamics, ensuring that land-use transitions are assessed not only at the landscape scale but also within individual field parcels, where management interventions occur.

3.3. R Data

The spatial pattern of rainfall erosivity (R factor) across the Myjava sub-basin for the 2011–2040 period reveals a distinct north–south gradient, with higher erosivity values concentrated in the northern and northeastern highlands and lower values toward the southern lowlands. The interpolated R values range from approximately 43 to 58 MJ·cm·ha^{-1}·h^{-1}·yr^{-1}, indicating moderate to high rainfall aggressiveness within the region. These gradients reflect strong influence by the basin's orographic configuration, where elevation and slope exposure enhance convective precipitation intensity and kinetic energy. This spatial heterogeneity in rainfall erosivity is an important control in the subsequent USLE-2D simulations, as it modulates the erosive potential of overland flow, particularly when interacting with steep slopes and exposed agricultural parcels. Areas exceeding 55 MJ·cm·ha^{-1}·h^{-1}·yr^{-1} may experience increased soil detachment rates, emphasizing the necessity of conservation practices in erosion-prone uplands (Figure 2).

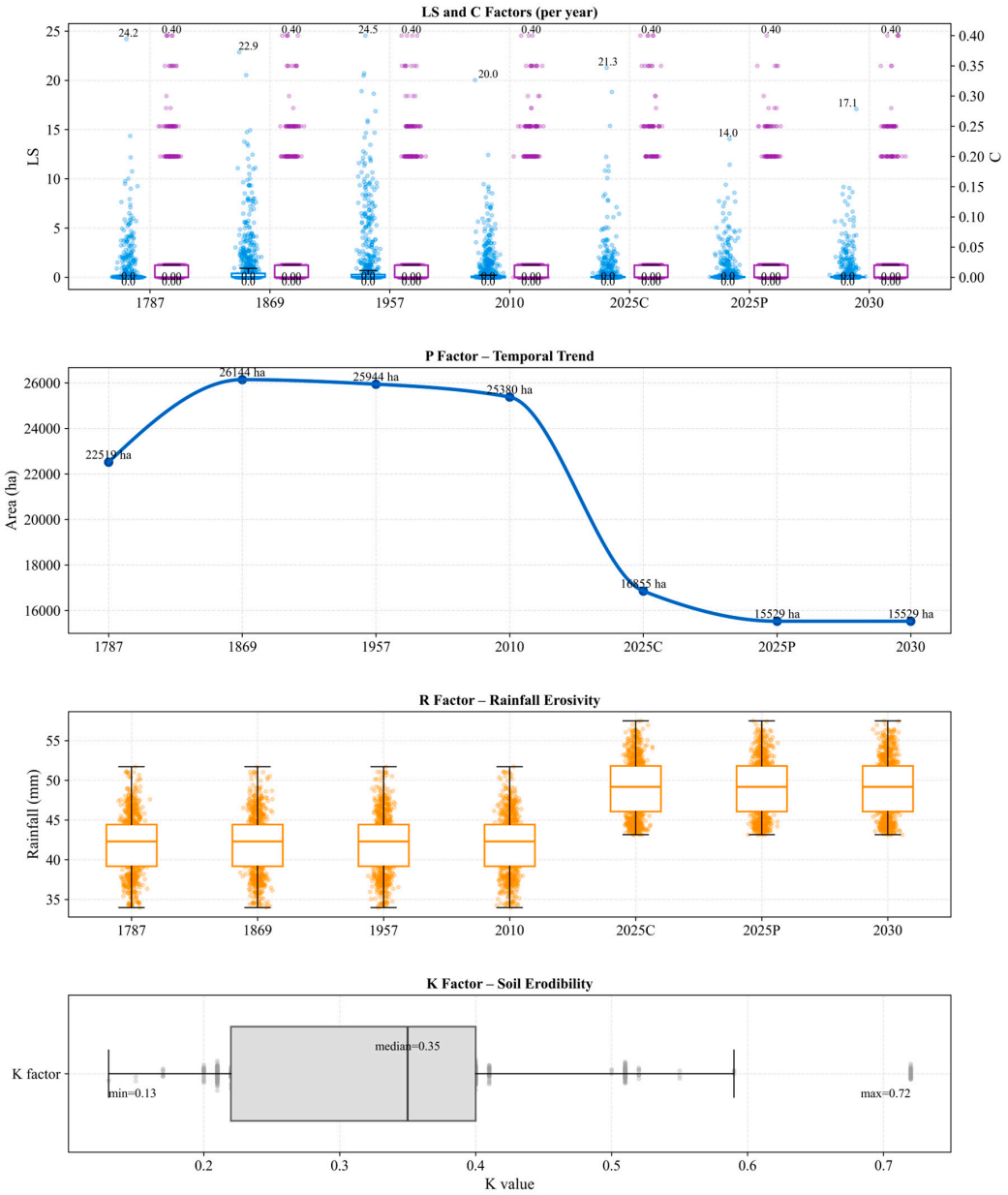

Figure 2. Temporal distribution and variability of key erosion-modelling factors (LS, C, P, R, and K) in the Myjava Basin (1787–2030). Blue symbols (LS and C graph) indicate the LS factor, and purple symbols indicate the C factor.

3.4. K Data

The spatial distribution of the soil erodibility factor (K) across the Myjava sub-basin shows marked heterogeneity, reflecting variations in soil texture, structure, and organic matter content that collectively determine the susceptibility of surface materials to detachment by rainfall and runoff. K values range from 0.13 to 0.72 (Figure 2). This intrinsic soil property contributes to the long-term spatiotemporal patterns of erosion intensity observed across the basin (Figure 3). Higher erodibility is observed predominantly in the central and southern parts of the basin (Figure 4), where shallow Cambisols and Luvisols dominate across steeper terrain. These soils exhibit weak structural stability and limited infiltration capacity, increasing their vulnerability to rill and interrill erosion. In contrast, lower K values occur in the western and lowland zones, where deeper and finer-textured soils with higher organic matter offer greater resistance to erosive forces. This spatial differentiation indicates that soil erodibility is a key intrinsic driver of erosion risk in the basin, modulating the response of the landscape to the combined effects of rainfall intensity and land-use change.

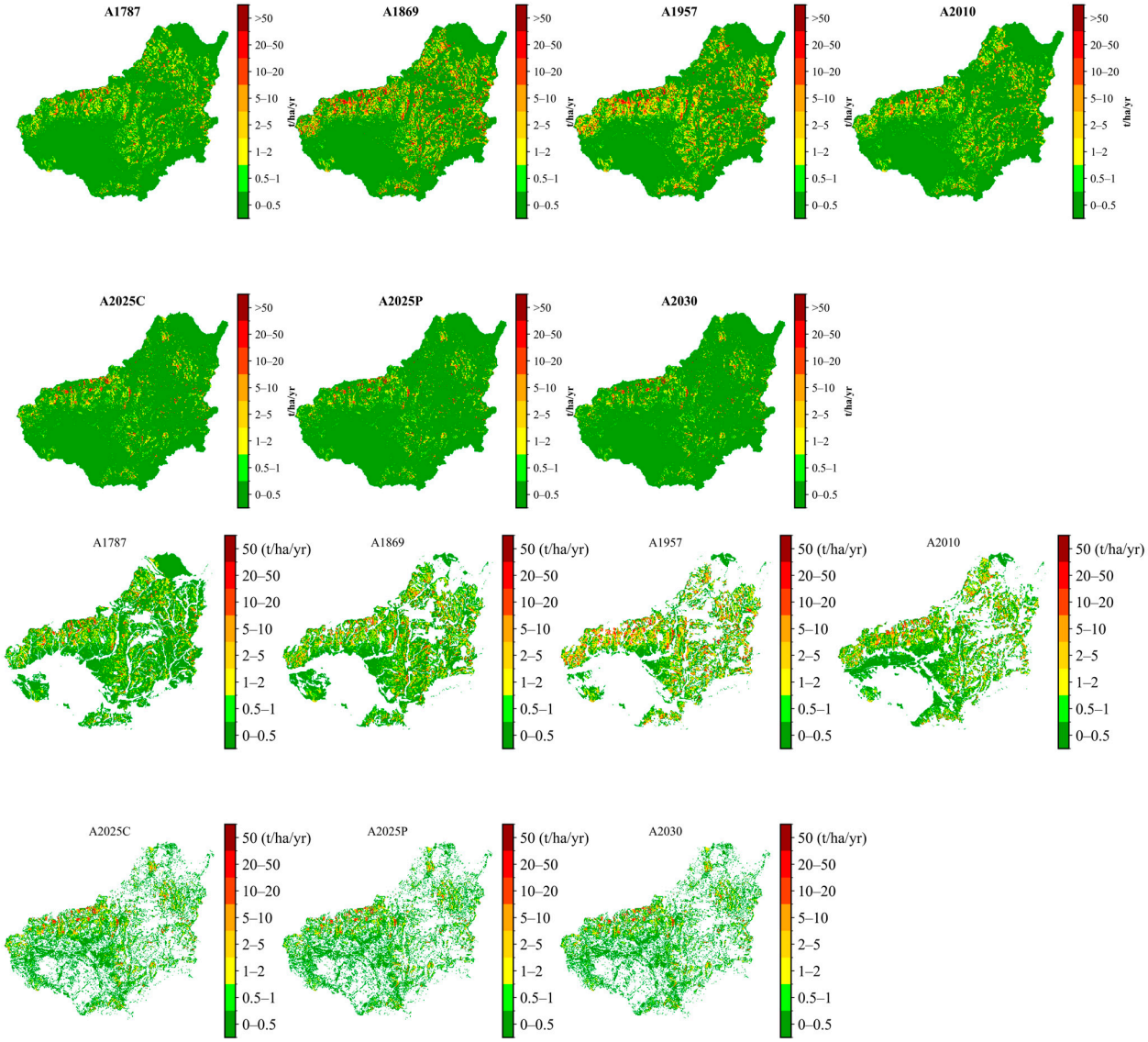

Figure 3. Spatiotemporal patterns of soil erosion intensity for all land-uses and arable lands in the Myjava Basin from 1787 to 2030, showing persistent erosion hotspots despite the overall decline.

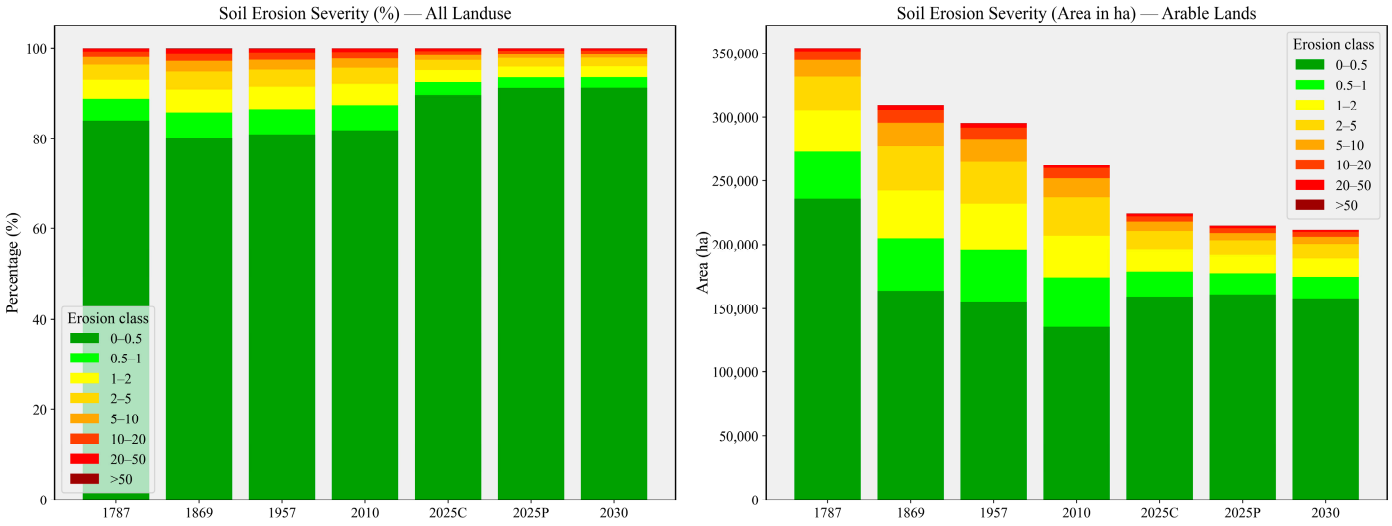

Figure 4. Temporal changes in soil erosion severity for all land-uses and arable lands in the Myjava Basin (1787–2030).

3.5. LS Data

The spatiotemporal distribution of the LS factor (ranging from 0 to 65) in the Myjava Basin between 1787 and 2030 clearly demonstrates the topographic control on erosion potential, exhibiting a consistent pattern that mirrors the basin's terrain morphology. Across all temporal layers, high LS values (shown in yellow to orange tones) are concentrated along steep slopes and deeply incised valleys, where increased flow accumulation and gradient enhance shear stress and soil detachment. Conversely, low LS values (depicted in green) dominate the gently undulating uplands and valley bottoms, where shorter slope lengths and mild gradients substantially reduce erosive energy. Despite extensive land-use transitions from 1787 through the projected 2025 and 2030 scenarios, the overall LS pattern remains relatively stable, reflecting the intrinsic and persistent role of topography in shaping the Myjava landscape. While land-use management and conservation practices can locally attenuate erosion rates, the enduring presence of high LS zones highlights the geomorphic dominance of slope form and relief as fundamental constraints governing spatial erosion dynamics within the basin (Figure 2).

3.6. C Data

The spatial distribution of the C factor in the Myjava Basin from 1787 to 2030 reveals a gradual and progressive improvement in vegetation cover and land management practices. In the historical periods (1787–1869), areas with higher C values (>0.3), depicted in orange and red, were widespread, particularly in agricultural zones vulnerable to surface runoff and soil disturbance (Figure 2). These regions indicate intensive land-use and limit protective vegetation. Over time, especially after 1957, the expansion of forests and the implementation of sustainable farming practices significantly reduced the extent of high C factor areas, while zones with low C values ($\leq$0.1), represented in grey and light green, became more dominant. By 2025 and 2030, both conservation (2025C) and projected (2025P, 2030) scenarios are predicted to show an increasingly stabilized landscape, characterized by extensive low C factor regions, suggesting enhanced vegetation cover and reduced erosion susceptibility. This temporal trend underscores the positive impact of reforestation, conservation tillage, and land-use policy strengthening ecological resilience and mitigating soil erosion risks within the Myjava Basin.

3.7. P Factor

In the Myjava sub-basin, the P factor, representing the effect of supporting conservation practices in the Universal Soil Loss Equation (USLE), was classified into the following two distinct categories: zero and one (Figure 2). Areas assigned a value of zero correspond to forests and other non-arable land-uses, where natural vegetation and ground cover effectively minimize runoff and soil detachment, thereby acting as intrinsic erosion control systems. Conversely, zones categorized as one represent arable lands, where tillage and reduced vegetation cover expose the soil to direct raindrop impact and surface flow, making them the primary contributors to sediment yield in the basin. This binary distinction in the P factor provides a simplified yet practical framework for identifying erosion-prone areas and underscores the critical role of land-use, particularly the balance between cultivated and forested areas, in governing the spatial variability of soil loss within the Myjava sub-basin.

3.8. Soil Erosion in Myjava Basin

The percentage distribution of soil erosion severity across all land-uses from 1787 to 2030 demonstrates a long-term structural stability in the landscape. Low-erosion categories (0–0.5 and 0.5–1 t ha^{-1} yr^{-1}) consistently dominate, representing roughly four-fifths of the entire area across all periods. Medium-severity classes (1–2 and 2–5 t ha^{-1} yr^{-1}) show slight but consistent contributions, indicating localized zones of moderate erosive response linked to terrain variation and land-use transitions. Importantly, the higher erosion classes (5–10, 10–20, 20–50, and >50 t ha^{-1} yr^{-1}) remain present throughout the timeline, although occupying relatively small fractions of land (<5%) (Figure 3). The persistence of these hotspots reflects inherent topographic constraints and rainfall-driven erosivity, which continue to shape erosion patterns even as land-use practices evolve. Ref. [31] similarly found that modelled erosion intensities in the Myjava Basin are strongly concentrated on steep convex hillslopes, confirming the persistent spatial clustering of erosion hotspots. Ref. [32]. Similar findings were reported for flood hazards in the upper Myjava Basin, where households identified rapid runoff from steep headwater slopes as a major contributor to local flood risk [33]. Comparable patterns of persistent sediment accumulation in small central European catchments were also reported by [8], highlighting how upstream erosion hotspots maintain long-term sediment delivery. Overall, the stability of both low- and high-severity percentages suggests that the fundamental geomorphic controls of the basin have remained influential and relatively stable for more than two centuries.

The erosion severity trends within arable lands show a clear long-term reduction in the total area affected, yet all erosion classes, from low to very high, remain present throughout the historical and projected periods (Figure 4). Low-severity categories (0–0.5 and 0.5–1 t ha^{-1} yr^{-1}) occupy the largest share of arable land, but the medium classes (1–2 and 2–5 t ha^{-1} yr^{-1}) also persist as substantial components of cultivated landscapes, reflecting the natural sensitivity of sloped agricultural fields (Figure 4). Notably, the higher erosion classes (5–10, 10–20, 20–50, and >50 t ha^{-1} yr^{-1}) experience marked reductions in area over time, especially after 1957, indicating the positive influence of improved soil conservation measures, crop cover management, and reduced cultivation on vulnerable terrains. By 2030, although the extent of high-severity zones is significantly smaller than in earlier centuries, their continued presence highlights that certain cultivated areas remain intrinsically erosion-prone and require sustained management attention. These patterns emphasize that arable land, while improving, continues to host the full spectrum of erosion risks, from minimal loss to severe degradation. Ref. [10] similarly emphasized that small reservoirs respond sensitively to changes in upstream erosion intensity, linking catchment-scale erosion dynamics with downstream flood-retention performance.

The long-term trajectory of soil erosion across the landscape reveals a distinct historical peak followed by progressive stabilization in both total erosion and average erosivity. Total erosion for all land-uses rises sharply between 1787 and 1869, reflecting a period when land clearing, population expansion, and early agricultural development increased hillslope exposure (Figure 5). A similar pattern is observed in arable lands, where erosion rates were exceptionally high during the pre-industrial and early agricultural phases, reaching their maximum in the nineteenth century. However, both datasets show a substantial decline from 1957 onward, suggesting that improvements in land-use regulation, vegetation recovery, and shifts toward more controlled agricultural practices have collectively contributed to reduced erosive pressure across the landscape. This convergence toward lower erosion rates indicates that, despite variations in land-use and management intensity, erosive forces have been mitigated through progressive changes in land management.

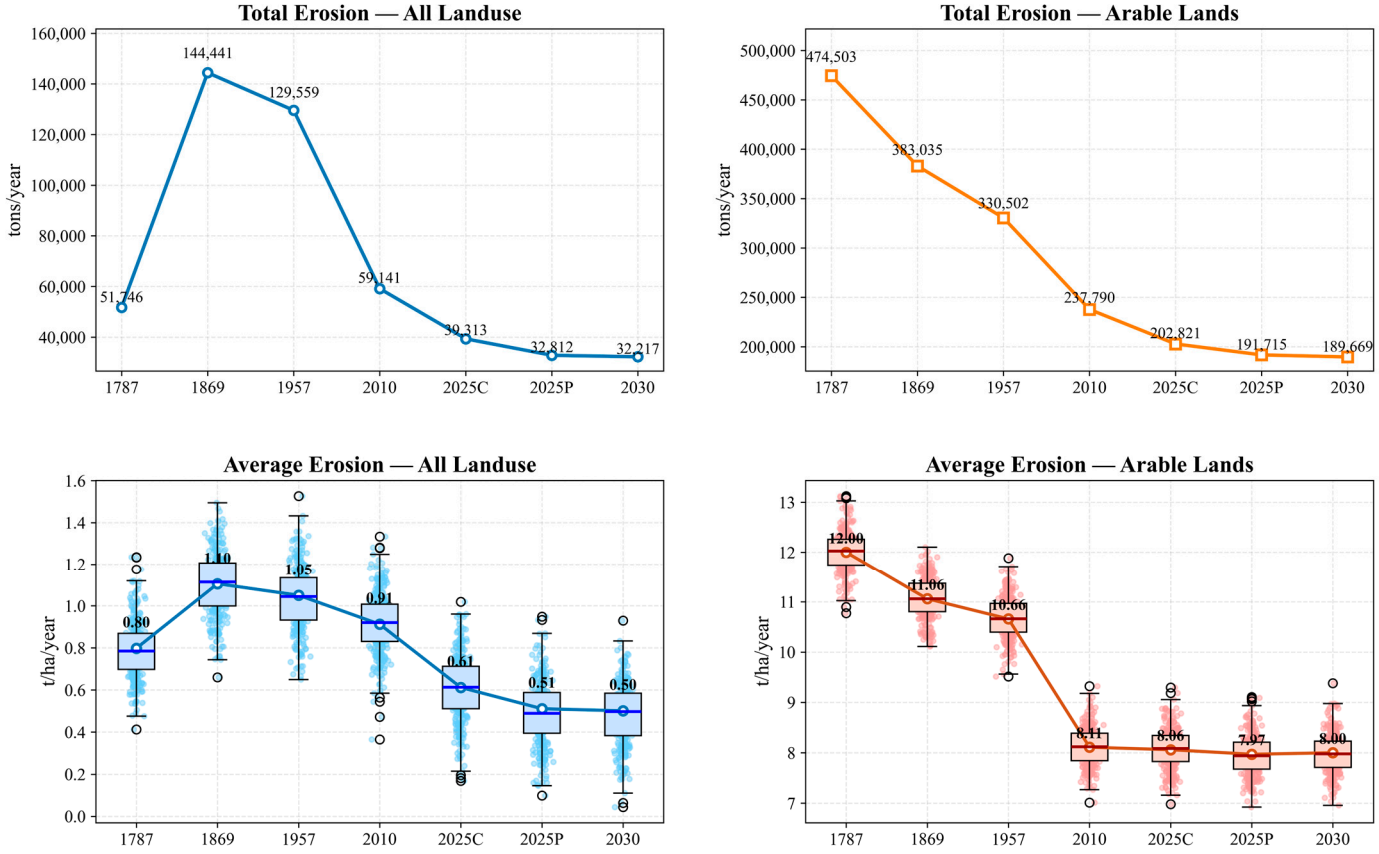

Figure 5. Temporal dynamics of total and average soil erosion for all land-uses and arable lands in the Myjava Basin (1787–2030).

Average (per-hectare) erosion provides complementary insight into total erosion patterns by highlighting persistent spatial differences in erosive stress across land-use types. Despite overall declines in total erosion, arable land consistently exhibits erosion rates several times higher than the landscape average throughout the study period, reflecting its inherent sensitivity to rainfall erosivity, topographic exposure, and soil disturbance. A marked reduction in average erosion after 1957, most pronounced in arable area, indicates the influence of improved cropping systems, enhanced soil cover, and early conservation practices. However, even under contemporary and projected scenarios, arable land remains disproportionately vulnerable compared to mixed land-use systems. Together, trends in total and average erosion reveal a long-term transition from earlier geomorphic-dominated degradation, amplified by rapid land opening, to modern erosion dynamics increasingly shaped by land-use planning and management interventions. While these measures have

improved overall landscape resilience, the continued susceptibility of arable land highlights the ongoing need for targeted soil conservation and adaptive management strategies.

3.9. Principal Component Analysis (PCA) Result Computation

Across the seven temporal datasets, the scree plot shows a stable variance structure dominated by the first two principal components in the Myjava Basin [30,34]. PC1 explains approximately 38–50% of the variance (44.97% in 1787; 49.78% in 1869; 48.73% in 1957; and 49.77% in 2010), declining in later scenarios to 38.35% in 2025C, 37.59% in 2025P, and 37.59% in 2030. This component is primarily controlled by LS and R factors [24], reflecting the persistent influence of topography and rainfall erosivity over more than two centuries [23]. PC2 consistently contributes 20–24% of variance (22.37% in 1787; 29.00% in 1869; 21.64% in 1957; 20.74% in 2010; and around 23.8% in future scenarios), capturing gradients linked to soil erodibility (K factor) and vegetation or land-cover conditions (C factor) [24]. Together, PC1 and PC2 explain more than 60–78% of total variance in all periods, indicating stable biophysical controls on erosion dynamics, see Figure 6.

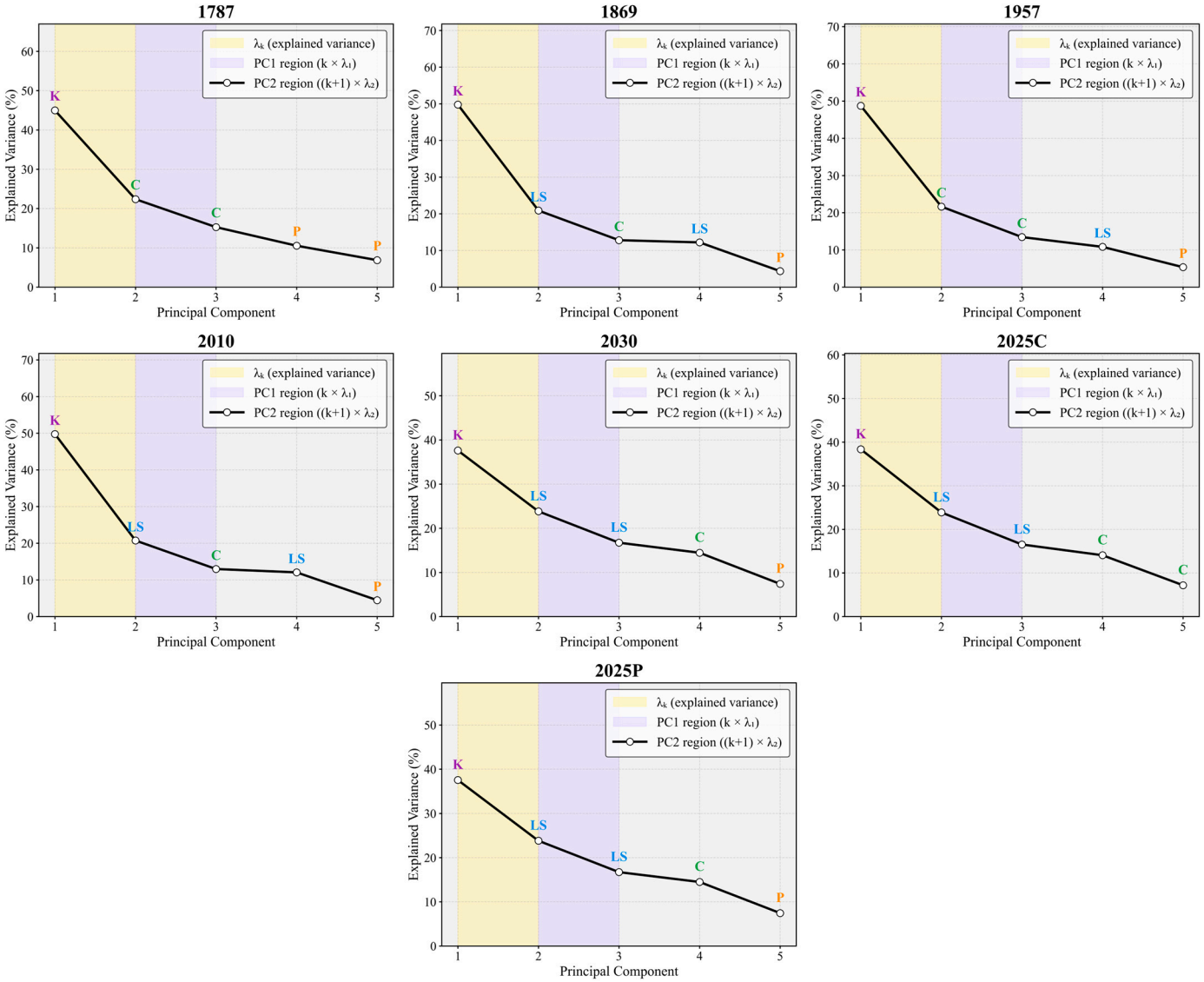

Figure 6. Explained variance of principal components for historical and projected erosion factors in the Myjava Basin (1787–2030).

Despite this overall stability, temporal shifts are evident. In 1787 and 1869, PC1 dominance (±45–50%) reflects landscapes primarily governed by natural gradients, whereas by 1957 and 2010, the increased contribution of PC2 highlights the growing influence of vegetation cover and land management practices [24]. In the projected scenarios of 2025C, 2025P, and 2030, PC1 falls below 40%, indicating a more balanced interaction among climatic, topographic, and anthropogenic factors. While the geomorphological framework remains a persistent structural control, contemporary and future erosion dynamics increasingly reflect integrated socio-ecological influences [35].

4. Discussion

4.1. Interpretation of PCA Variance Structure and Dominant Erosion Factors

The PCA loading patterns provide a more detailed understanding of how specific environmental variables contribute to the dominant gradients revealed by PC1 and PC2. Across the historical timeline, PC1 is consistently characterized by strong positive loadings from rainfall erosivity (R) and slope length–steepness (LS), confirming their role as the primary biophysical forces shaping erosional susceptibility. These two factors jointly encode the long-term geomorphic control of the basin, where steep terrain and climatic energy interact to define the structural predisposition to soil loss. Meanwhile, K factor (soil erodibility) and C factor (vegetation cover) typically load more strongly on PC2, suggesting that these variables modulate, rather than dictate, the sensitivity imposed by the dominant physical processes. This separation between PC1 and PC2 loadings highlights the hierarchical nature of erosion drivers, with macro-scale geomorphic–climatic forces operating at the core, and soil-vegetation conditions influencing the landscape's response capacity (Figure 7).

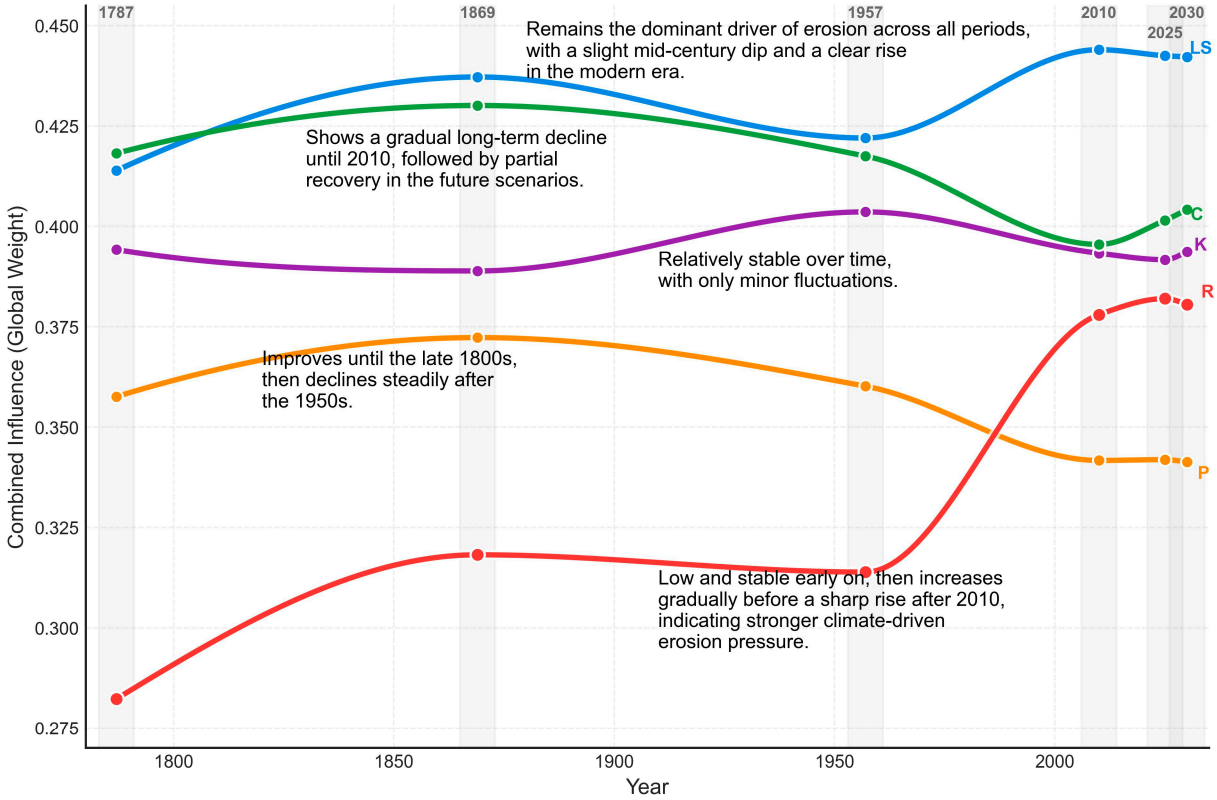

Figure 7. Long-term dynamics of PCA-derived erosion factors in the Myjava Basin (1787–2030).

Over time, the loading matrices reveal a gradual redistribution of influence among variables, reflecting changes in vegetation structure and evolving land-use practices. Early

periods such as 1787 and 1869 show loadings overwhelmingly dominated by R and LS, consistent with landscapes minimally influenced by management practices. By 1957 and 2010, the increasing magnitude of the C and P loadings signals a shift in which vegetation cover, agricultural practices, and management interventions begin to exert measurable influence on erosional dynamics (Figure 8). This transition becomes more pronounced in future scenarios (2025C, 2025P, and 2030), where the loadings reveal a more balanced interplay of climatic, topographic, and human-driven factors. Such redistribution indicates that while the geomorphological template remains stable, the system shows increasing sensitivity to anthropogenic modification. Thus, PCA loadings complement the scree plots by showing not how much variance is explained, but which variables structurally define that variance, providing a mechanistic link between long-term environmental forcing and changing management conditions. This long-term consistency in PCA structure underscores that multi-century analysis is essential to distinguish persistent geomorphic controls from shorter-term land-use signals that are often emphasized in decadal erosion studies.

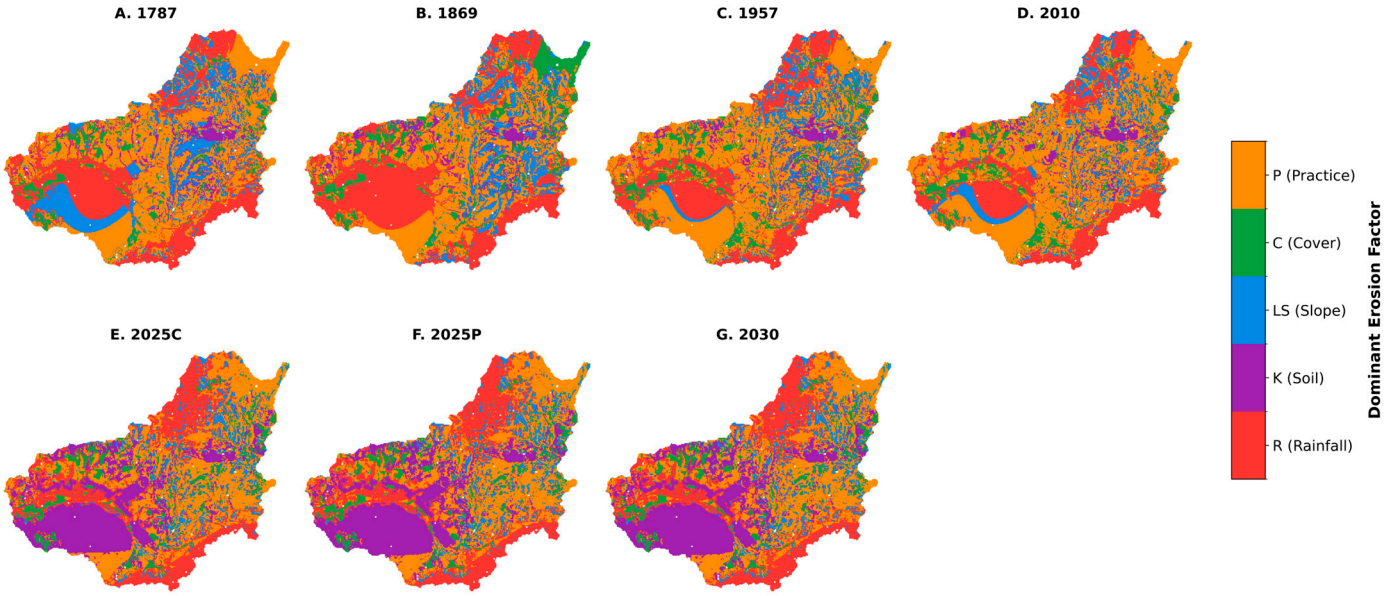

Figure 8. Dominant erosion factor maps derived from PCA for the Myjava Basin (1787–2030).

4.2. Additional Insights from PCA Biplots

The PCA biplots integrate the information from both the variance structure (scree plots) and the variable contributions (loading tables) into a single visual representation, allowing the relationships between time periods, erosion factors, and their multivariate patterns to be examined simultaneously. In these biplots, the orientation and length of each variable vector reflect both its direction of influence and its relative strength in shaping the principal component space. Consistent with earlier findings, R and LS appear as long vectors aligned closely with the PC1 axis, indicating their dominant contribution to the primary geomorphic gradient. Conversely, variables such as C and P tend to align toward PC2, demonstrating their role in representing variation in vegetation cover and land management. The position of each year within this multivariate space illustrates how the erosion environment shifts over time, from earlier periods situated near the R–LS axis to later periods drifting toward the C–P direction, capturing changes in the relative influence of erosion-related drivers (Figure 9).

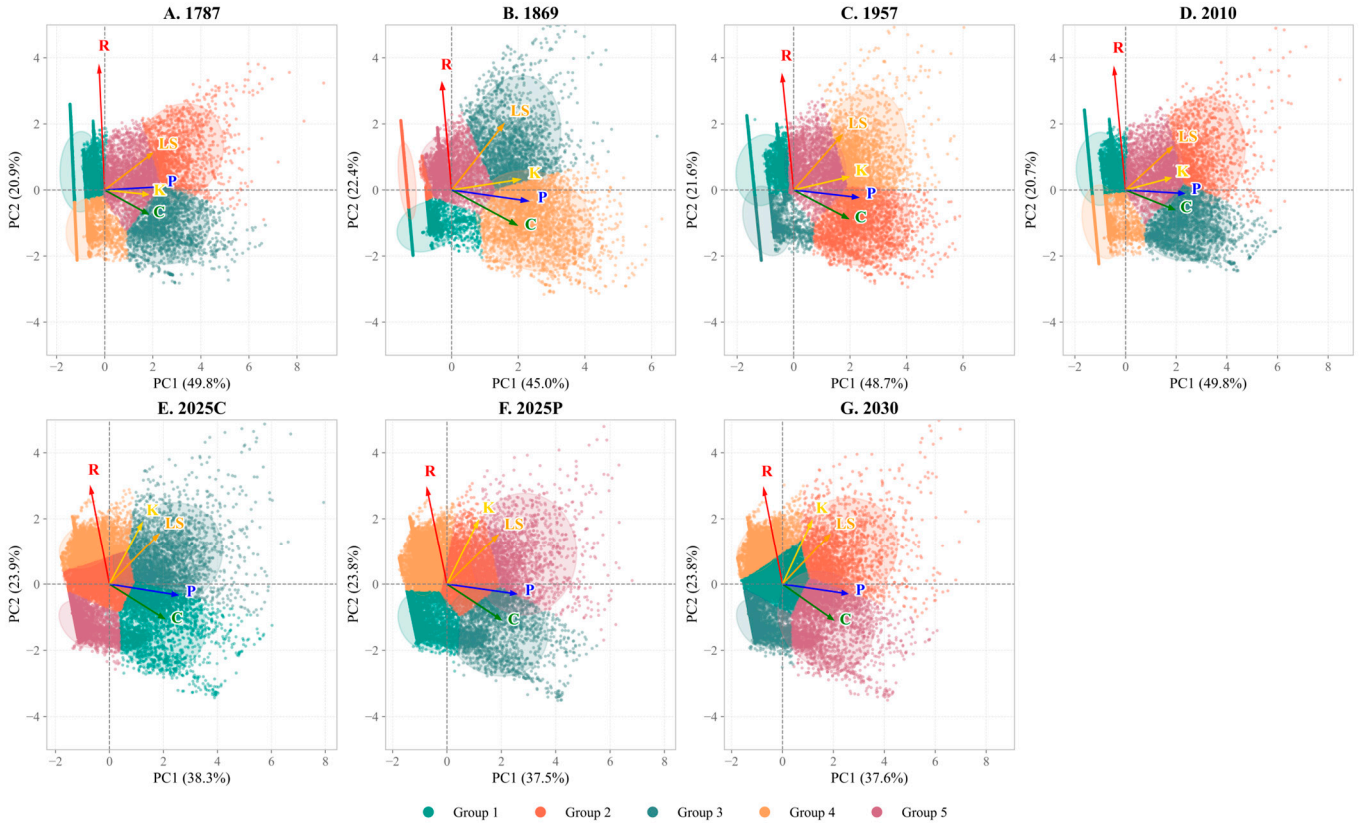

Figure 9. PCA biplots of erosion factors (R, K, LS, C, and P) for historical and projected periods in the Myjava Basin (1787–2030).

Across the timeline, the biplots further reveal how individual years cluster according to the prevailing erosion regimes. Earlier landscapes (1787, 1869) cluster tightly along vectors associated with strong natural erosive forces, reflecting steep slopes and high rainfall erosivity. Transitional years such as 1957 and 2010 move toward the centre of the plot, representing the mixed influences of geomorphic controls and changing land-use conditions. Future projections (2025–2030) appear positioned closer to the C and P vectors, implying a landscape where vegetation cover and management-related factors represent a greater share of total variance. The biplot therefore synthesizes the entire PCA structure, showing not only which forces dominate but how their combined effects evolve over time. In doing so, it reinforces the interpretation that erosion dynamics arise from a shifting balance between persistent geomorphological memory and changes in land management and vegetation cover.

Taken together, the scree plots, loading matrices, and PCA biplots converge toward a coherent interpretation of the long-term erosion dynamics across the study landscape. The scree plots consistently indicate that the first two principal components explain the majority of variance in all time periods, demonstrating the presence of stable, overarching gradients that govern erosion susceptibility. The loading matrices clarify the nature of these gradients, showing that geomorphic and climatic drivers, particularly rainfall erosivity (R) and slope characteristics (LSs), are historically the dominant forces shaping the landscape, while management-related variables such as C and P have gained influence in the more recent periods. Similar multidecadal PCA assessments in mountain watersheds have shown that slope-driven geomorphic controls and rainfall erosivity consistently dominate the principal components, while management factors gradually rise in influence during recent land-use transitions [36]. The PCA biplots further reinforce this interpretation by visually illustrating how the multivariate structure of the erosion environment evolves

over time, with earlier years clustering near strong natural erosive forces and later years shifting toward vectors associated with vegetation cover and conservation interventions. PCA-based spatial analyses of ecosystem disturbance similarly reveal marked temporal shifts in multivariate structure, with early conditions dominated by natural geomorphic climatic drivers and later periods reflecting increasing influence from vegetation recovery and landscape management processes [37].

Despite the apparent differences across the three analytical products, the combined evidence reveals a consistent temporal storyline as follows: the landscape retains a strong geomorphological baseline shaped by long-term physical processes, yet land-use increasingly modulates erosion patterns as land-use intensifies and management strategies evolve. The divergence seen across methods is therefore not a contradiction but a complementarity; each analysis highlights a different dimension of the same environmental reality. Together, they offer a robust and multidimensional understanding of how natural and human factors interact to drive erosion risk across historical, contemporary, and projected future scenarios. Related dimensionality-reduction studies in river-basin landscapes likewise demonstrate that separating natural climatic geomorphic controls from anthropogenic land-use influences yields clearer diagnostic insight into long-term landscape responses, reinforcing the interpretive power of multivariate frameworks for complex environmental systems [38]. This integrative perspective strengthens confidence in the interpretation and underscores the value of PCA as a comprehensive framework for diagnosing complex land degradation processes.

4.3. Influence of Land-Use Dynamics on Soil Erosion Processes

Transitions in land-use modify erosion processes by simultaneously altering the C and P factors and the hydrologic pulse that activates them [7]. Comparable process-based responses to land-cover transitions have been documented in temperate European hilly landscapes, where changes in vegetation cover and management alter runoff generation, sediment connectivity, and the effective C × P protection of cultivated slopes [1].

In landscapes like Myjava, where cropland persists on long convex slopes and valley shoulders, shifts from annual crops toward grassland or forest systematically dampen interrill and rill detachment, not only through canopy and litter but also via changes in roughness and flow connectivity at field edges. Similar evidence from European loess and hilly agricultural catchments indicates that sustained vegetation recovery and conservation practices reduce soil loss by lowering runoff energy and interrupting slope connectivity [5]. Ref. [36] similarly demonstrated that crop management strategies in Myjava region can substantially reduce sediment transport and flood-related erosion on hilly agricultural land. This finding is consistent with field-based and catchment-scale studies in Slovakia, which documented how crop management, sediment connectivity, and reservoir sedimentation jointly regulate erosion and sediment delivery in small hilly catchments, including the Myjava region [7–10]. While these Slovak studies primarily reported sediment yield or deposition volumes rather than spatially explicit erosion rates, their results indicate that erosion is concentrated on steep cultivated slopes, consistent with the average arable-land erosion rates simulated in this study (approximately 12 $t \cdot ha^{-1} \cdot yr^{-1}$ in the late 18th century, declining to about 8 $t \cdot ha^{-1} \cdot yr^{-1}$ in recent and projected periods).

Reservoir-based studies further support this mechanism by quantifying sediment delivery from small central European catchments and demonstrating the value of sediment archives for evaluating catchment-scale erosion signals [8]. Independent model validation using bathymetric sediments also confirms that erosion-model outputs can be constrained against observed sedimentation in Slovak conditions [9]. Likewise, joint assessments of sed-

imentation and flood retention in Slovak small reservoirs highlight how land management and catchment connectivity shape sediment pathways [10].

Recent field-to-catchment assessments show that parcel-based implementations of RUSLE capture these connectivity effects as follows: when the cropland mosaic fragments and perennial cover expand, sediment sources contract and delivery pathways break, yielding measurable drops in modelled soil loss even where topography (LS) remains intrinsically high. In the central European context, this mechanism is consistent with documented management effects on sediment transport and flood-related erosion in hilly agricultural land, including Myjava region [7].

Yet land-use trajectories unfold under a moving climate baseline as follows: intensifying convective rainfall can re-energize otherwise "stabilized" hillslopes. Previous Slovak and central European assessments indicate that rainfall erosivity (R) varies over time and can influence absolute erosion magnitudes, particularly on steep cultivated parcels. For central Europe, and Myjava region specifically, projections and high-resolution rain analyses indicate rising rainfall erosivity (R), with the northern uplands flagged for the largest increases; this means that cropland retained on steep parcels may remain disproportionately hazardous even as regional reforestation proceeds [11]. Although abandonment and secondary forest recovery tend to reduce average soil loss, but hotspots persist where high LS combines with cropland and limited conservation practice under increasingly intense rainfall. The most resilient futures therefore pair land-use transitions that privilege perennial cover in slope-intensive units with targeted conservation on any remaining arable strips, an approach consistent with recent catchment experiments showing that reducing structural connectivity is as decisive as lowering plot-scale erodibility [12]. By integrating multi-century land-use trajectories with spatially explicit erosion modelling, this study demonstrates that land-use interventions reduce average erosion rates but do not fully override long-term geomorphic controls, a distinction that cannot be resolved by short-term or event-based erosion assessments.

While continental-scale assessments across Europe provide critical benchmarks on soil erosion under land-use and climate change, e.g., [39], such approaches necessarily rely on generalized inputs and coarse spatial representations that cannot resolve parcel-level heterogeneity, long-term land-use legacies, or uncertainties in individual erosion factors. Global syntheses further document the widespread nature of soil and water degradation worldwide, but similarly emphasize the need for regional, spatially explicit analyses to capture local processes and management effects. In this context, regional parcel-based studies are essential to understand how multi-century land-use dynamics interact with topography, management, and changing rainfall erosivity to shape erosion responses.

4.4. Model Integration and Uncertainty in Spatiotemporal Erosion Assessment

The integration of land-use projection models with physically based formulations like USLE-2D provides a complementary framework for long-term landscape assessments. Ref. [9] showed that model reliability increases when erosion estimates are cross-validated with empirical sediment measurements, such as bathymetric surveys. Each method carries distinct epistemic assumptions, with machine learning approaches capturing empirical spatial patterns while process-based formulations retain mechanistic fidelity. Their combination allows soil erosion to be represented using both data-driven and process-oriented perspectives. In the Myjava Basin, where long historical data coexist with detailed parcel-level mapping, this duality enhances the capacity to simulate long-term patterns of erosion and recovery. Yet, such integration also magnifies uncertainty. Spatial misalignment between datasets, the temporal granularity of land-use transitions, and the stochastic nature of rainfall erosivity all propagate error through the modelling chain [1,2]. Recognizing and

quantifying these uncertainties through ensemble modelling, sensitivity testing, and cross-validation across historical baselines is therefore a necessary step for ensuring transparency and robustness in model interpretation.

4.5. Limitations

A key limitation arises from the heterogeneity of historical land-use sources. Because land-use maps from 1787 to 1957 were generated using different cartographic techniques and classification schemes, the internal consistency of the dataset cannot be fully guaranteed. Such methodological discrepancies may introduce positional uncertainty and classification bias that propagate into both USLE-2D and land-use projection simulations, particularly along arable–non-arable boundaries. In addition, the standardization of historical land-use into arable and non-arable categories necessarily simplifies structural differences among vegetation types and cropping systems, which may mask finer-scale variability in canopy structure, litter cover, and management intensity relevant to C–P parameterization. Additionally, key drivers of erosion such as river network evolution, hydrological connectivity, and transportation corridors could not be incorporated into earlier temporal layers due to the absence of reliable historical records. Their omission represents a structural constraint in reconstructing past erosion processes, particularly in valley systems where channel proximity strongly shapes sediment pathways. Local geomorphic changes such as gully incision, terracing, or small-scale sediment redistribution may have modified slope length and steepness at fine spatial scales; however, due to the absence of reliable historical elevation data, these dynamics could not be reconstructed and are therefore not represented in the LS factor, which is treated as a stable geomorphic template at the catchment scale.

Recent methodological advances emphasize that integrating multi-source data (e.g., satellite time series, DEM derivatives, and socio-environmental variables), together with probabilistic approaches, can reduce uncertainty and enhance model transferability [6,11,12,39]. Explicitly acknowledging data and model limitations therefore remains essential, as no single method can fully represent landscape complexity [13].

This study has several limitations that should be acknowledged. First, historical land-use maps (1787–1957) were produced using different cartographic techniques and classification schemes, which may introduce inconsistencies in long-term LULC trajectories. Second, although slope and rainfall erosivity are well-represented, other important drivers such as hydrological connectivity, drainage network evolution, and historical road density could not be incorporated due to the unavailability of reliable past spatial data. These omissions likely cause a conservative estimation of localized erosion hotspots. Soil erodibility (K) was assumed to be temporally static due to the lack of spatially explicit historical soil data, which may affect absolute erosion magnitudes over the long term. The C and P factors were parameterized using time-invariant, representative values for each land-use state, which do not capture seasonal vegetation dynamics or the varying effectiveness of specific conservation practices, potentially affecting absolute erosion estimates. USLE-2D outputs could not be directly calibrated or validated against field-measured erosion or sediment data due to the lack of continuous historical observations, which limits quantitative assessment of absolute erosion magnitudes. Third, model integration between land-use projections and USLE-2D carries compounded uncertainties from each methodological step, and although patterns are consistent with regional geomorphic theory, absolute erosion values should be interpreted with caution, whereas relative spatial patterns and temporal differences among scenarios are considered robust due to the consistent modelling framework and harmonized inputs. Future work should integrate hydrological datasets, high-resolution historical DEMs, and multi-source environmental archives to reduce these uncertainties.

5. Conclusions

This study demonstrates how 240 years of land-use change have shaped soil erosion dynamics in the Myjava Basin by integrating parcel-level historical reconstructions with USLE-2D modelling. The long-term reconstruction shows a marked decline in arable land alongside the expansion of grassland and forest cover, yet erosion hotspots persisted on steep agricultural slopes due to enduring LS and rainfall erosivity controls. Model outputs show that low-erosion classes dominate throughout the timeline, whereas high-severity zones gradually diminish but never disappear, confirming the geomorphic constraints governing erosion risk. PCA further reveals a stable hierarchical structure in which LS and R drive the primary variance, while soil properties and vegetation–management factors increasingly influence erosion patterns in later periods. This multivariate structure highlights that long-term geomorphic controls remain dominant, while land-use and management practices modulate erosion magnitude rather than fully overriding physical constraints. Although uncertainties arise from heterogeneous historical land-use sources, differences in data scale, and compounded modelling steps, the overall trends indicate a long-term stabilization of the landscape, tempered by persistent local vulnerabilities. Accordingly, absolute erosion values should be interpreted with caution, whereas relative spatial patterns and temporal differences among scenarios are considered robust due to the consistent modelling framework and harmonized inputs. Together, these results provide a coherent understanding of how geomorphology and evolving land-use practices interact to regulate erosion risk across historical, contemporary, and projected scenarios.

Author Contributions: Conceptualization, K.H., S.K., R.V., and M.D.; Methodology, A.N.P., K.H., and R.V.; Software, A.N.P. and R.V.; Validation, A.N.P., R.V., and M.D.; Formal Analysis, A.N.P.; Investigation, A.N.P. and R.V.; Resources, R.V., M.D., and K.H.; Data Curation, A.N.P. and R.V.; Writing—Original Draft Preparation, A.N.P.; Writing—Review and Editing, A.N.P., R.V., M.D., K.H., and S.K.; Visualization, A.N.P.; Supervision, S.K. and K.H.; Project Administration, S.K.; Funding Acquisition, K.H. and S.K. All authors have read and agreed to the published version of the manuscript.

Funding: This research was funded by the Slovak Research and Development Agency under contract numbers APVV 23-0332 and VV-MVP-24-0208, and by the VEGA Grant Agency under grant number 1/0657/25.

Data Availability Statement: The data presented in this study are available on request from the corresponding author. The datasets generated and analyzed in this study are not publicly available due to institutional restrictions and ongoing research use. The data are part of a larger research project and are still being utilized for subsequent studies. Access to the data may be granted upon reasonable request and with permission from the data provider.

Conflicts of Interest: The authors declare no conflicts of interest. The funders had no role in the design of the study; in the collection, analyses, or interpretation of data; in the writing of the manuscript; or in the decision to publish the results.

Abbreviations

The following abbreviations are used in this manuscript:

ANN	Artificial Neural Network
ASCII	American Standard Code for Information Interchange
BPEJ	Bonitované Pôdno-Ekologické Jednotky (Soil–Ecological Quality Units, Slovakia)
CA	Cellular Automata
CAP	Common Agricultural Policy (European Union)
C Factor	Cover Management Factor (USLE/RUSLE)

DEM	Digital Elevation Model
GIS	Geographic Information System
ha	Hectare
K Factor	Soil Erodibility Factor (USLE/RUSLE)
L Factor	Slope Length Factor (USLE/RUSLE)
LS Factor	Slope Length–Steepness Factor (USLE/RUSLE)
LULC	Land-Use and Land Cover
m a.s.l.	Metres Above Sea Level
MJ	Megajoule
P Factor	Support Practice Factor (USLE/RUSLE)
PCA	Principal Component Analysis
Pg yr^{-1}	Petagrams per Year
R Factor	Rainfall Erosivity Factor (USLE/RUSLE)
RUSLE	Revised Universal Soil Loss Equation
S Factor	Slope Steepness Factor (USLE/RUSLE)
S-JTSK	Slovenský Jednotný Trigonometrický Systém (Slovak National Coordinate System)
TIN	Triangulated Irregular Network
USLE	Universal Soil Loss Equation
USLE-2D	Two-Dimensional Universal Soil Loss Equation
Z-score	Standardized Score for Normalization

References

1. Borrelli, P.; Robinson, D.A.; Panagos, P.; Lugato, E.; Yang, J.E.; Alewell, C.; Wuepper, D.; Montanarella, L.; Ballabio, C. Land use and climate change impacts on global soil erosion by water (2015–2070). *Proc. Natl. Acad. Sci. USA* **2020**, *117*, 21994–22001. [CrossRef]
2. Panagos, P.; Borrelli, P.; Meusburger, K.; Alewell, C.; Lugato, E.; Montanarella, L. Estimating the soil erosion cover-management factor at the European scale. *Land Use Policy* **2015**, *48*, 38–50. [CrossRef]
3. Kumar, Y.; Kumar, S.; Kaushik, N.; Prakash, V.; Garg, K.; Nalia, M.; Ghosh, S. Recent advancements in climate change projections and socioeconomic scenarios used to evaluate climate impacts and adaptation measures. In *Agriculture Toward Net Zero Emissions*; Elsevier: Amsterdam, The Netherlands, 2025; pp. 425–440. [CrossRef]
4. Valent, P.; Výleta, R. Estimating Rainfall Erosivity Factor Using Future Climate Projection in the Myjava Region (Slovakia). *Acta Hortic. Et Regiotect.* **2021**, *24*, 31–36. [CrossRef]
5. Maliariková, M. Analýza zmien využitia územia pre odhad ich vplyvu na zmeny odtokového režimu v poľnohospodársky využívanom povodí. Ph.D. Thesis, Slovenská Technická Univerzita v Bratislave, Bratislava, Slovakia, 2024.
6. Valent, P.; Rončák, P.; Maliariková, M.; Behan, Š. Utilization of Historical Maps in the Land Use Change Impact Studies: A Case Study from Myjava River Basin. *Slovak J. Civ. Eng.* **2016**, *24*, 15–26. [CrossRef]
7. Hlavčová, K.; Danáčová, M.; Kohnová, S.; Szolgay, J.; Valent, P.; Výleta, R. Estimating the effectiveness of crop management on reducing flood risk and sediment transport on hilly agricultural land—A Myjava case study, Slovakia. *Catena* **2019**, *172*, 678–690. [CrossRef]
8. Honek, D.; Michalková, M.Š.; Smetanová, A.; Sočuvka, V.; Velísková, Y.; Karásek, P.; Konečná, J.; Németová, Z.; Danáčová, M. Estimating sedimentation rates in small reservoirs—Suitable approaches for local municipalities in central Europe. *J. Environ. Manag.* **2020**, *261*, 109958. [CrossRef]
9. Németová, Z.; Honek, D.; Kohnová, S.; Hlavčová, K.; Michalková, M.Š.; Sočuvka, V.; Velísková, Y. Validation of the EROSION-3D Model through Measured Bathymetric Sediments. *Water* **2020**, *12*, 1082. [CrossRef]
10. Valent, P.; Výleta, R.; Danáčová, M. A Joint Sedimentation-Flood Retention Assessment of a Small Water Reservoir in Slovakia: A New Hope for Old Reservoirs? *Geosciences* **2019**, *9*, 158. [CrossRef]
11. Toková, L.; Hološ, S.; Šurda, P.; Kollár, J.; Lichner, Ľ. Impact of Duration of Land Abandonment on Infiltration and Surface Runoff in Acidic Sandy Soil. *Agriculture* **2022**, *12*, 168. [CrossRef]
12. Assede, E.S.P.; Orou, H.; Biaou, S.S.H.; Geldenhuys, C.J.; Ahononga, F.C.; Chirwa, P.W. Understanding Drivers of Land Use and Land Cover Change in Africa: A Review. *Curr. Landsc. Ecol. Rep.* **2023**, *8*, 62–72. [CrossRef]
13. Selmy, S.A.H.; Kucher, D.E.; Mozgeris, G.; Moursy, A.R.A.; Jimenez-Ballesta, R.; Kucher, O.D.; Fadl, M.E.; Mustafa, A.-R.A. Detecting, Analyzing, and Predicting Land Use/Land Cover (LULC) Changes in Arid Regions Using Landsat Images, CA-Markov Hybrid Model, and GIS Techniques. *Remote. Sens.* **2023**, *15*, 5522. [CrossRef]

14. Vîrghileanu, M.; Săvulescu, I.; Mihai, B.; Bizdadea, C.; Paraschiv, M. RUSLE-based scenarios for sustainable soil management: Case studies from Romanian Subcarpathians. *Eur. J. Soil Sci.* **2024**, *75*, e13526. [CrossRef]
15. Munteanu, C.; Kuemmerle, T.; Keuler, N.S.; Müller, D.; Balázs, P.; Dobosz, M.; Griffiths, P.; Halada, L.; Kaim, D.; Király, G.; et al. Legacies of 19th century land use shape contemporary forest cover. *Glob. Environ. Change* **2015**, *34*, 83–94. [CrossRef]
16. Špaček, Š. Seamless vector map 50. *Kartogr. Listy* **1999**, *7*, 71–74. (In Slovak)
17. Lapin, A.; Paaschen, T.; Junghans, K.; Lübbert, A. Bubble column fluid dynamics, flow structures in slender columns with large-diameter ring-spargers. *Chem. Eng. Sci.* **2002**, *57*, 1419–1424. [CrossRef]
18. Faško, P.; Handžák, Š.; Šrámková, N. Number of days with snow cover and its average height 1:2,000,000. In *Landscape Atlas of the Slovak Republic*; Miklós, L., Hrnčiarová, T., Eds.; Slovak Environmental Agency: Bratislava, Slovakia, 2002; Volume 99.
19. Malíšek, A. Evaluation of the erosion effectiveness factor of a downpour. *Geogr. časopis* **1990**, *42*, 410–422. (In Slovak)
20. Onderka, M.; Pecho, J. Update of the erosive rain factor in Slovakia using data from the period 1961–2009. *Contrib. Geophys. Geod.* **2019**, *49*, 355–371. [CrossRef]
21. Wischmeier, W.H.; Smith, D.D. *Predicting Rainfall Erosion Losses: A Guide to Conservation Planning*; Handbook No. 537; The USDA Agricultural: Beltsville, MD, USA, 1978.
22. Govers, G. Rill erosion on arable land in central Belgium: Processes and limiting factors. *Catena* **1991**, *18*, 133–145. [CrossRef]
23. McCool, D.K.; Brown, L.C.; Foster, G.R.; Mutchler, C.K.; Meyer, L.D. Revised Slope Steepness Factor for the Universal Soil Loss Equation. *Trans. ASAE* **1987**, *30*, 1387–1396. [CrossRef]
24. Renard, K.G. *Predicting Soil Erosion by Water: A Guide to Conservation Planning with the Revised Universal Soil Loss Equation (RUSLE)*; United States Government Printing: Washington, DC, USA, 1997.
25. Nearing, M.A. A Single, Continuous Function for Slope Steepness Influence on Soil Loss. *Soil Sci. Soc. Am. J.* **1997**, *61*, 917–919. [CrossRef]
26. Li, W.; Li, P.; Yan, L.; Hu, J.; Wang, L.; Li, D.; Dan, Y.; Huang, L.; Zhao, G. Impacts of spatial resolutions of UAV-LiDAR-derived DEMs on erosion modelling in the hilly and gully Loess Plateau. *Catena* **2025**, *255*, 109059. [CrossRef]
27. Zhang, J.X.; Chang, K.; Wu, J.Q. Effects of DEM resolution and source on soil erosion modelling: A case study using the WEPP model. *Int. J. Geogr. Inf. Sci.* **2008**, *22*, 925–942. [CrossRef]
28. Alewell, C.; Borrelli, P.; Meusburger, K.; Panagos, P. Using the USLE: Chances, challenges and limitations of soil erosion modelling. *Int. Soil Water Conserv. Res.* **2019**, *7*, 203–225. [CrossRef]
29. Gessler, P.E.; Moore, I.D.; McKenzie, N.J.; Ryan, P.J. Soil–landscape modelling and spatial prediction of soil attributes. *Int. J. Geogr. Inf. Syst.* **1995**, *9*, 421–432. [CrossRef]
30. Putra, A.N.; Jaenudin; Prasetya, N.R.; Sugiarto, M.T.; Sudarto; Prayogo, C.; Maritimo, F.; Admajaya, F.T. Utilizing Remote Sensing and Random Forests to Identify Optimal Land Use Scenarios and Address the Increase in Landslide Susceptibility. *Sustainability* **2025**, *17*, 4227. [CrossRef]
31. Németová, Z.; Honek, D.; Látková, T.; Michalková, M.Š.; Kohnová, S. An assessment of soil water erosion in the Myjava hill land: The application of a physically-based erosion model. *Pollack Period.* **2018**, *13*, 197–208. [CrossRef]
32. Nosko, R.; Maliariková, M.; Brziak, A.; Kubáň, M. Formation of Gully Erosion in the Myjava Region. *Slovak J. Civ. Eng.* **2019**, *27*, 63–72. [CrossRef]
33. Solín, Ľ.; Madajová, M.S.; Michaleje, L. Flood hazards in the headwaters area: Lessons learned from a survey of households in the upper Myjava basin, Slovakia. *Water Policy* **2017**, *19*, 1081–1096. [CrossRef]
34. Jolliffe, I.T.; Cadima, J. Principal component analysis: A review and recent developments. *Philos. Trans. R. Soc. A Math. Phys. Eng. Sci.* **2016**, *374*, 20150202. [CrossRef]
35. Yu, B.; Chen, F.; Xu, C. Landslide detection based on contour-based deep learning framework in case of national scale of Nepal in 2015. *Comput. Geosci.* **2020**, *135*, 104388. [CrossRef]
36. Manojlović, S.; Sibinović, M.; Srejić, T.; Novković, I.; Milošević, M.V.; Gatarić, D.; Carević, I.; Batoćanin, N. Factors Controlling the Change of Soil Erosion Intensity in Mountain Watersheds in Serbia. *Front. Environ. Sci.* **2022**, *10*, 888901. [CrossRef]
37. Toosi, N.B.; Soffianian, A.R.; Fakheran, S.; Waser, L.T. Waser, Mapping disturbance in mangrove ecosystems: Incorporating landscape metrics and PCA-based spatial analysis. *Ecol. Indic.* **2022**, *136*, 108718. [CrossRef]
38. Kang, Y.; Wang, Z.; Xu, B.; Shen, W.; Chen, Y.; Zhou, X.; Liu, Y.; Zhang, T.; Wang, G.; Jia, Y.; et al. Disentangling the Response of Vegetation Dynamics to Natural and Anthropogenic Drivers over the Minjiang River Basin Using Dimensionality Reduction and a Structural Equation Model. *Forests* **2024**, *15*, 1438. [CrossRef]
39. Panagos, P.; Ballabio, C.; Himics, M.; Scarpa, S.; Matthews, F.; Bogonos, M.; Poesen, J.; Borrelli, P. Projections of soil loss by water erosion in Europe by 2050. *Environ. Sci. Policy* **2021**, *124*, 380–392. [CrossRef]